

Breaking BEC: the fast and the quantum

A. Kovtun, ^{a,b} **M. Zantedeschi**^{a,b}

^a*Max-Planck-Institut für Physik,
Föhringer Ring 6, D-80805, München, Germany*

^b*Arnold Sommerfeld Center, Ludwig-Maximilians-Universität,
Theresienstraße 37, 80333, München, Germany*

E-mail: akovtun@mpp.mpg.de, michaelz@mpp.mpg.de

ABSTRACT: In this work we numerically explore the quantum behaviour of a classically unstable relativistic Bose-Einstein condensate (BEC). The main goal is to study the phenomenon of so-called quantum break-time which amounts to a significant departure from a classical description. It has been suggested previously that the existence of Lyapunov instability is crucial for a fast quantum breaking, chaos and scrambling. In order to clarify the issue, we work within the 2-PI effective action formalism and introduce a simple and universal criterion of quantum breaking. We indeed observe that the fast quantum break-time is controlled by the Lyapunov exponent of the unstable BEC.

KEYWORDS: Bose-Einstein condensate, Bright Soliton, Quantum break-time, Scrambling, Non-perturbative effects, 2PI effective action, Black-Holes

Contents

1	Introduction	1
1.1	Recipe for deriving the quantum break time	3
2	Theory Setup	5
2.1	Condensate	5
2.2	Bright Soliton	6
2.3	2PI effective action	8
2.4	Saddle solution as initial condition	9
3	Numerical Analysis	10
3.1	Evolution along the BEC trajectory	11
3.2	Quantum break time	13
4	Conclusions and Outlook	14

1 Introduction

Quantum breaking is the idea that a given classical solution, due to its quantum nature, might not be eternally faithful in describing the evolution of a system. In fact, due to quantum effects, the system might deviate, in time, from the classical trajectory and significantly change its structure, therefore making the aforementioned solution eventually unreliable. The concept that macroscopic objects can become quantum after a certain critical time-scale was first introduced and developed in a series of papers [1–4] motivated by a microscopic composite picture of a black hole, and it was later generalized to various systems, such as inflationary cosmologies and axion field [5, 6]. The outcome of these studies was that certain macroscopic systems, that are usually assumed to be well-described classically, in reality, exhibit a rather short quantum break-time. There is a class of systems that seem to exhibit breaking much faster than the others.

Namely, in [7] the connection between the phenomenon of quantum breaking and chaos was established and it was argued that a many-body macroscopic system can undergo a maximally fast quantum breaking and become chaotic, provided it possesses a Lyapunov exponent γ , with the following formula for quantum break-time:

$$t_{qb} \sim \gamma^{-1} \log N, \tag{1.1}$$

where N is a certain macroscopic particle number. In [7], this equation was explicitly checked on an example of a 1 + 1 dimensional system with Lyapunov exponent, namely a non relativistic unstable BEC. The above mentioned quantity was derived by means of entanglement arguments. In this paper it was also suggested that quantum breaking and

chaos represent the microscopic mechanisms behind the so-called phenomenon of quantum information scrambling and that the existence of Lyapunov exponent is crucial for a system to saturate the logarithmic bound on the fast scrambling time proposed in [8]. It is argued that these kind of systems are the ones which break the fastest.

The results of [7] leaves certain open questions. For example, it is unclear whether relativistic corrections would affect the above predicted timescale.

The purpose of this article is therefore to study these relativistic effects. Due to the absence of particle conservation, it is rather natural to expect a similar behaviour under the replacement $N \rightarrow Q$ which is the conserved charge of the system in the relativistic case. This is anyway absolutely not obvious, as the relativistic theory possess a much wider spectrum. However, we verify in this work, that a very similar law as (1.1) holds for a relativistic model endowed with $U(1)$ symmetry and attractive self-interaction i.e. we check that the quantum break time is given by

$$t_{qb} = \gamma^{-1} \log Q + \text{constant}, \quad (1.2)$$

where Q is the full charge of the BEC, γ is the Lyapunov exponent associated with the system and the small constant presence will be shown to be related to the chosen criterion used to extract t_{qb} . Moreover note how this timescale happen to be infinite in the semi-classical limit (namely as $\hbar \rightarrow 0$, $t_{qb} \rightarrow \infty$), therefore ensuring the captured effect to be genuinely quantum and not visible classically.

To obtain it we work in the semi-classical framework of 2PI effective action. In fact, with this method, we are able to study the unitary Minkowski-time evolution of a quantum coherent state mimicking a relativistic Bose-Einstein condensate. In turn, this allows us to check how the system dynamically deviates from the classical condensate solution. To do so, we introduce a universal criterion which can be easily applied to find quantum breaking. Namely, we look at the dynamical evolution of the conserved integral quantity constraining the system i.e. charge. Indeed, as discussed below, such quantity is exactly conserved due to Noether's theorem. However, since we are working within the 2PI framework, such composite quantity receives two contributions from the one- and the two-point expectation values respectively (note that these quantities balance each other out because of the above mentioned symmetry to each loop order in case of an \hbar expansion [9]). We will refer to the former as classical charge Q_{cl} and to the latter as quantum charge Q_q . At the beginning of the evolution, the distribution of charge between Q_{cl} and Q_q is fixed by initial conditions. As one would expect, for a coherent state describing a classical configuration, we have that $Q_{cl} \gg Q_q$. However, as the system evolves, this needs not be the case anymore. It is therefore natural to define quantum breaking as the timescale when the two above-mentioned quantities become comparable. A great advantage from this criterion is obtained, as no need to deal with rescattering effects at the microscopic level is necessary, although one could infer it from the diagrams retained within a given 2PI expansion scheme. It is worth mentioning that in principle different integral quantities could serve as a mean to estimate the quantum break time as long as their conservation constrains the dynamics of the system. For example, one could equally look at energy or, in case of a non-relativistic system, to occupation number. In the present article, however, our main focus is charge

since, as we will see below, the contributions from the 1 and the 2 point expectation values, split in a very clear and easy manner.

We have already applied in [10] this approach to the study of the relativistic BEC with repulsive self-interaction and studied the dependence of quantum break-time on the charge of initial coherent state. Although, we did not extract analytical dependence, it is apparent that for extremely big and extremely small charges, quantum break-time is at least polynomial, and matters on very long timescales. We would like to draw the reader attention to the observation that in case of cosmic axion [6] the quantum break time is as well polynomial in the number of constituents initially accumulated in the condensate, although in that case, it is derived by means of perturbative calculations. No conflict between our and their result was found. We therefore conclude that our newly introduced simple criterion universalizes the notion of quantum breaking, as not only it is applicable to a wide class of systems, but it also agree with the quantum breaking timescale derived with different methods in the literature (based on perturbative calculation in [6] and based on scrambling in [7]).

Before moving forward and explain more in depth the chosen quantum breaking criterion for this particular model, we would like to underline that the evolution, as well as the considered initial conditions, are translation invariant. This, in turn, does not allow a genuine classical localised instability to come into play.

1.1 Recipe for deriving the quantum break time

Before moving to the main part of the article it is worth explaining our setup as well as how (1.2) was obtained.

Within the 2PI framework we studied the behaviour of an $SO(2)$ symmetric scalar field theory with attractive quartic coupling in $1 + 1$ dimension. To obtain its Minkowski time evolution, we derived the equations of motion (e.o.m.) from the 2PI action $\Gamma[\phi, G]$ using the Schwinger-Keldysh time contour, therefore obtaining a fully causal dynamics [11–13]. In turn, this opened the question of a proper choice of initial conditions for the 1 and 2 point function ϕ and G . For this purpose we chose the stationary solution at tree-level which is given by a condensate whose frequency we will denote by $\omega \in (0, m)$. For fixed spatial length L , as ω is decreased, the condensate solution becomes eventually classically unstable. In this region, fluctuations, and correspondingly G , grow exponentially, leading to a very fast quantum breaking. To evaluate the deviations from the classical stationary solution we proceeded as in [10], namely we took advantage of the $SO(2)$ associated conserved charge given by [10]:

$$Q = \int d\mathbf{x} \lim_{y \rightarrow x} \epsilon_{ab} \partial_{x^0} \left(\phi_a(x) \phi_b(y) + G_{ab}(x, y) \right), \quad (1.3)$$

where ϵ_{ab} is 2-dimensional Levi-Civita tensor and $d\mathbf{x}$ denotes integration over spatial coordinates. From (1.3) we observe that two contributions make up for the total conserved charge. For later convenience we split these up and name them as *classical* $Q_{cl}(t)$ and

quantum $Q_q(t)$ charges:

$$Q_{cl}(x^0) = \int_0^L dx^1 \lim_{y \rightarrow x} \epsilon_{ab} \partial_{x^0} \phi_a(x) \phi_b(y) = \int_0^L dx^1 \left(\dot{\phi}_1(x) \phi_2(x) - \dot{\phi}_2(x) \phi_1(x) \right), \quad (1.4)$$

$$Q_q(x^0) = \int_0^L dx^1 \lim_{y \rightarrow x} \epsilon_{ab} \partial_{x^0} F_{ab}(x, y). \quad (1.5)$$

Here, we recall from [13]

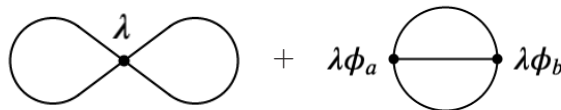
$$G_{ab}(x, y) = F_{ab}(x, y) - \frac{i}{2} \text{sgn}_{\mathcal{C}}(x^0 - y^0) \rho_{ab}(x, y),$$

with F_{ab} (ρ_{ab}) corresponding to the anti-commutator (commutator) expectation value and $\text{sgn}_{\mathcal{C}}(t)$ is the sign function along some time contour \mathcal{C} , which in this problem we choose to be Schwinger-Keldysh contour. Notice that Q_{cl} corresponds to the standard Noether charge, while Q_q is a new contribution that follows from our choice to work within the 2PI framework. Due to the above mentioned initial conditions, $Q_{cl}(t=0) \gg Q_q(t=0)$ [10]. Note that at $t_{initial}$, the leading contribution to the dynamic is therefore due to the rescattering of the highly occupied zero momentum modes described by ϕ into G . However, since Q_q is determined by G , the classical instability leads to a fast growth of Q_q . We therefore look at how the ratio $Q_q(t)/Q_{cl}(t)$ evolves in time. This will serve as a mean to measure the departure from the initial configuration. In fact, it is natural to define the quantum break time as the moment when

$$Q_q(t_{qb}) \simeq Q_{cl}(t_{qb}). \quad (1.6)$$

We therefore use (1.6) as a way to estimate the quantum break time.

Before moving forward it is worth explaining the limits of the approximations employed in the 2PI effective methods. In the following simulations we expanded Γ up to the second order in loops. This corresponds to the inclusion of the following diagrams:



$$\text{Figure-eight loop with } \lambda \text{ at vertex} + \lambda \phi_a \text{ --- } \text{Bubble diagram with } \lambda \phi_b \text{ at vertices} \quad (1.7)$$

where λ is the quartic coupling. For in depth discussion of how these two diagrams emerge in the effective action see [10]. What is relevant in the present discussion is their relevance w.r.t. the dynamics. While the first one is a local diagram, and therefore a trivial correction to the e.o.m., the second one is responsible for the interaction between ϕ and G . Such a diagram, as long as we are in the perturbative regime, and $t < t_{qb}$, is the most relevant one for the dynamics and the one responsible for quantum breaking. Note, however, that after t_{qb} , rescattering effects between non zero modes might become of comparable importance and, therefore, higher order in the loop expansion should be taken into account. It is worth stressing, anyway, that the above discussion implies that the two-loop approximation is

enough to reliably obtain the quantum break time via condition (1.6). Finally, note that the second diagrams scales schematically as $\lambda(\lambda\phi^2/m^2)$ which is exactly the necessary effective coupling that was used to capture quantum breaking in [5].

The remainder of this article is organized as follows: in the next section the theoretical setup and tools necessary to the analysis are introduced. In Sec. 3 the numerical results are analysed and discussed. Sec. 4 sums up our work, and outlines our conclusions.

2 Theory Setup

In this section we introduce the model and analyse it classically. Two distinct stable solutions are found in the spectrum depending on the classical frequency ω and the box size L : namely a condensate and a bright soliton. The transition point between the two corresponds to the appearance of an instability mode for the condensate.

Consider a real scalar field with attractive quartic self-interaction in a 1+1 dimensional finite box of size L endowed with $SO(2)$ global symmetry. The action of this theory is:

$$S[\varphi_a] = \int dx \left(\frac{1}{2}(\partial_\mu\varphi_a)^2 - \frac{1}{2}m^2\varphi_a^2 + \frac{\lambda}{16}(\varphi_a^2)^2 \right). \quad (2.1)$$

with $\lambda > 0$. Rescaling the field as

$$\varphi_a(t, x) = \sqrt{2}R(\omega t)_{ab} \tilde{f}_b(x), \quad (2.2)$$

where $R(\theta)$ is the usual $O(2)$ rotation matrix, and after fixing $\tilde{f}_b(x) = (f(x), 0)^T$, the equation of motion becomes:

$$\frac{d^2 f}{dx^2} + (\omega^2 - m^2) f + \frac{\lambda}{2} f^3 = 0, \quad (2.3)$$

supplemented with periodic boundary conditions.

Two solutions to (2.3) can be found: namely a homogeneous one, the condensate, and a localized one, the bright soliton [14]. In the following their relation and stability are discussed.

2.1 Condensate

Similarly to the repulsive case, the condensate solution is given by the homogeneous configuration:

$$f(x) = \sqrt{\frac{2(m^2 - \omega^2)}{\lambda}}, \quad (2.4)$$

where frequency covers the range $\omega \in (0, m)$. For this solution integrals of motion are

$$E_{b.c.} = \int dx \left[\frac{1}{2}(\dot{\varphi}_a)^2 + \left(\frac{d\varphi_a}{dx} \right)^2 + \frac{1}{2}m^2\varphi_a^2 - \frac{\lambda}{16}(\varphi_a^2)^2 \right] = \frac{L}{\lambda} (m^4 + 2m^2\omega^2 - 3\omega^4), \quad (2.5)$$

$$Q_{b.c.} = \int dx [\dot{\varphi}_1(x)\varphi_2(x) - \dot{\varphi}_2(x)\varphi_1(x)] = \frac{4\omega L(m^2 - \omega^2)}{\lambda}. \quad (2.6)$$

Notice that for this attractive interaction, the energy of the configuration is lower than the one of free particles, i.e. $E(\omega) \leq mQ(\omega)$ ¹. Moreover, since the potential for this model is unbounded from below², it is natural to question the classical stability of the system. To do so, we look at the spectrum of classical perturbations which is given by (see [10]):

$$\gamma_+(p_n) = \sqrt{p_n^2 + 3\omega^2 - m^2 + \sqrt{m^4 - 6m^2\omega^2 + 4p_n^2\omega^2 + 9\omega^4}}, \quad (2.7)$$

$$\gamma_-(p_n) = \sqrt{p_n^2 + 3\omega^2 - m^2 - \sqrt{m^4 - 6m^2\omega^2 + 4p_n^2\omega^2 + 9\omega^4}}, \quad (2.8)$$

where

$$p_n = \frac{2\pi n}{L} \quad (2.9)$$

Note that for solution (2.4), one perturbation mode is classically gapless i.e. $\gamma_-(0) = 0$. Therefore, to analyse the instability, we focus on the non zero modes. In particular, from (2.8), the first mode turning imaginary, as ω decreases, is p_1 at

$$\omega = \omega_{cr} = \sqrt{m^2 - \frac{2\pi^2}{L^2}}. \quad (2.10)$$

We therefore conclude that the condensate solution is classically stable for $\omega \in [\omega_{cr}, m)$ and unstable otherwise. We will see later in the analysis that the imaginary part of this mode $\text{Im}(\gamma_-(p_1))$ is the Lyapunov exponent. This situation reflects the presence of a Jeans instability and as size gets bigger more modes become unstable. It occurs successively, namely, a given mode p_n becomes unstable at $\omega_{cr}(p_n) = \sqrt{m^2 - 2\pi^2 n^2 / L^2}$. So, we can deduce that for fixed size L there will be $\lfloor mL / \sqrt{2}\pi \rfloor$ unstable modes.

2.2 Bright Soliton

In the non relativistic limit, the classical bright soliton was studied in [14] and its low lying spectrum beyond Bogolubov approximation near the point of phase transition was investigated in [16]. Here we focus on the relativistic case.

The solution is showed, for different ω 's, in fig. 1 and is given by

$$f(x) = \frac{4K(\mu)}{L\sqrt{\lambda}} dn\left(2K(\mu) \frac{x}{L} \middle| \mu\right), \quad (2.11)$$

where $K(\mu)$ is the elliptic integral of the first kind, $dn(x|\mu)$ is the jacobi elliptic function and μ is fixed by the condition

$$4K(\mu)^2(2 - \mu) = L^2(m^2 - \omega^2), \quad (2.12)$$

¹Here we mean by rest mass of the free particle the mass parameter in the Lagrangian, but one has to remember that if mass parameter is defined at infinite volume by means of conditions $\Sigma(m^2) = 0$ and $d\Sigma/dp^2(m^2) = 0$, than in finite volume it gets modified [15]. But as long as mass acquires an exponentially small correction we don't bother ourselves considering it.

²This plays no role in our analysis, because field amplitude is lower than $2m/\sqrt{\lambda}$ and we do not enter the domain when boundlessness can not be ignored anymore. In the general case, of course theory can be made bounded by means of inclusion of higher order terms, which can appear after integrating out some other fields

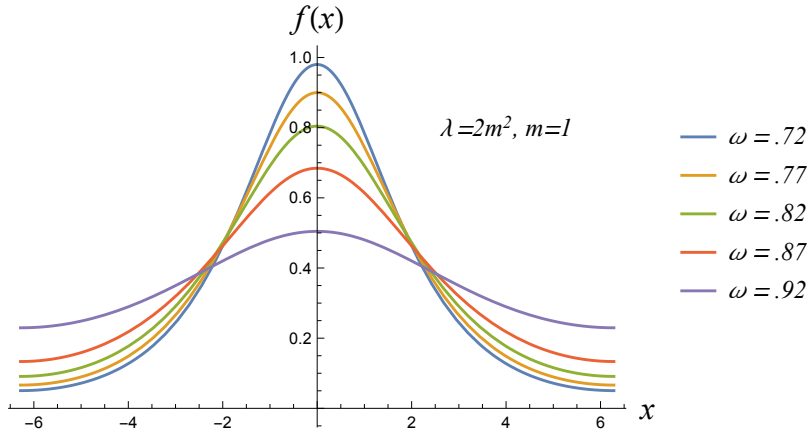


Figure 1. Bright soliton solution for different frequencies ω and length $L = 4\pi m^{-1}$.

for which a solution exists if $\omega \in (0, \omega_{cr})$. We would like to notice here that frequency at which solitonic solution appears in the spectrum is exactly the same frequency (2.10) when the first momentum mode becomes unstable. Therefore at ω_{cr} the spectrum splits. We also would like to draw reader's attention to the fact that in the relativistic model as ω approaches zero, bright soliton becomes unstable, branch of stable Q-balls continuously turns to the branch of unstable Q-clouds at the cusp point in contrary to the non-relativistic case.

The integrals of motion corresponding to bright soliton are:

$$E_{b.s.}(\omega) = \frac{16(4(\mu-1)K(\mu)^4 + L^2(4\omega^2 + 2)K(\mu)E(\mu))}{3\lambda L^3}, \quad (2.13)$$

$$Q_{b.s.}(\omega) = \frac{32\omega}{L\lambda}E(\mu)K(\mu). \quad (2.14)$$

where $E(\mu)$ is the elliptic integral of the second kind and $\mu = \mu(\omega)$ is given by (2.12).

To sum up, we have the following situation: for $\omega \in [\omega_{cr}, m)$ the condensate solution is classically stable and unique for equation (2.3). In this region, the collective coupling, proportional to $(\lambda/m^2)f^2$, increases as ω decreases. Upon reaching ω_{cr} a phase transition takes place. In this sense, the collective coupling is strong enough as to allow for a localization of the solution. Correspondingly, the fluctuations on top of the condensate display at least an unstable mode indicating the fact that, for a given fixed charge, there exists a classical configuration with lower energy (as it can be seen from comparing (2.5) and (2.13)).

The above statement can easily be deduced from figure 2. As it is possible to see, the soliton trajectory emerges from the branching point ω_{cr} . Moreover, as ω decreases (and the collective coupling increases), the soliton configuration localizes more and more up to the point where it becomes classically unstable. This happens in correspondence of ω_{cusp} which is the value for which the known instability condition is fulfilled [17, 18]:

$$\left. \frac{dQ_{cl}}{d\omega} \right|_{\omega=\omega_{cusp}} < 0. \quad (2.15)$$

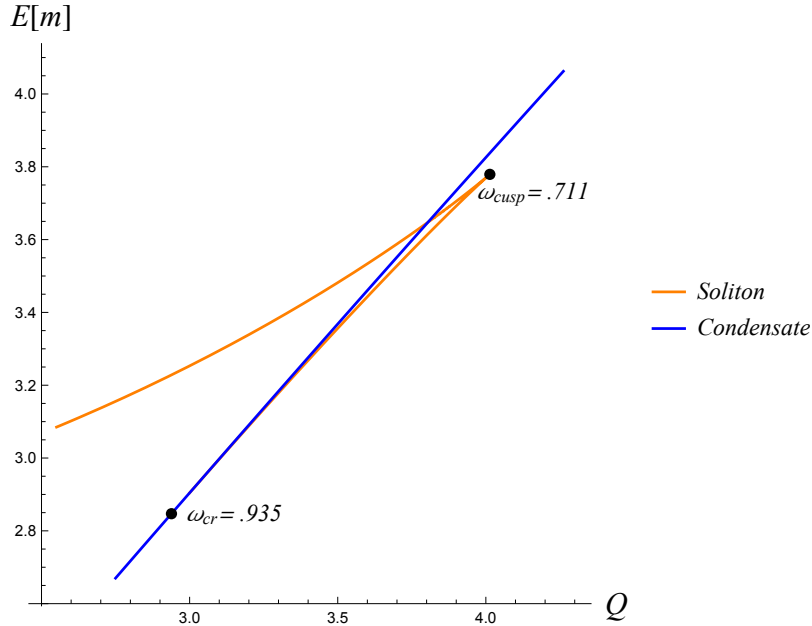


Figure 2. Energy versus charge behaviour of condensate and soliton. Here $L = 4\pi m^{-1}$ and $\lambda = 2m^2$.

For lower ω 's, the soliton solution corresponds to the points of the upper branch of Fig. 2.

Before moving forward it is important mentioning that although the potential is unbounded from below for the condensed (soliton), one can easily see from (2.4) ((2.11)), that the only source of classical instability under small perturbations is given by (2.10) ((2.15)). Moreover, notice that tunneling phenomena are not relevant in our quantum study as they are exponentially suppressed, while we will see that quantum breaking happens exponentially fast.

2.3 2PI effective action

Most of the notions in this section are already explained in depth in [10]. Here we report the main steps to establish notation. The 2PI effective action is given by

$$\Gamma[\phi, G] = S[\phi] + \frac{i}{2} \text{tr} \ln G^{-1} + \frac{i}{2} \text{tr} (G_0^{-1} G) + \Gamma_2[\phi, G] \quad (2.16)$$

where ϕ and G are correspondingly the 1 and 2 point Green's function expectation value and $\Gamma_2[\phi, G]$ is the sum of vacuum-vacuum 2-particle irreducible diagrams computed with vertices and propagators obtained from the shifted action. Upon stationarization, the equations of motion are obtained:

$$\begin{cases} \frac{\delta S[\phi]}{\delta \phi_a(x)} + \frac{i}{2} \text{tr} \left(\frac{\delta G_0^{-1}}{\delta \phi_a(x)} G \right) + \frac{\delta \Gamma_2[\phi, G]}{\delta \phi_a(x)} = 0 \\ G_{ab}^{-1}(x, y) - G_{0ab}^{-1}(x, y) + 2i \frac{\delta \Gamma_2[\phi, G]}{\delta G_{ab}(x, y)} = 0 \end{cases} \quad (2.17)$$

In order to solve these equations, it should be decided up to which order in \hbar we would like to approximate the dynamics. As explained above, for the purpose of this work it is enough to work up to two loops. Hence, $\Gamma_2[\phi, G]$ up to order \hbar^2 is given by (1.7).

In order to solve (2.17), another ingredient is necessary, namely the choice of the time contour. As in [10], we work here in the Schwinger-Keldysh formalism [11, 12]. In this way, the eom's derived from the stationarization of the 2PI effective action, are guaranteed to be causal, therefore allowing for an easier numerical implementation. Moreover, it is easier to rewrite the eom's by splitting the propagator in commutator and anticommutator contributions as:

$$G_{ab}(x, y) = F_{ab}(x, y) - \frac{i}{2} \text{sgn}_{\mathcal{C}}(x^0 - y^0) \rho_{ab}(x, y), \quad (2.18)$$

$$F_{ab}(x, y) = \frac{1}{2} \langle \{ \phi_a(x), \phi_b(y) \} \rangle, \quad (2.19)$$

$$\rho_{ab}(x, y) = i \langle [\phi_a(x), \phi_b(y)] \rangle, \quad (2.20)$$

where the $\text{sgn}_{\mathcal{C}}(x^0 - y^0)$ is taken along the in-in time contour and guaranties proper time ordering. Here, $F_{ab}(x, y)$ is known as statistical propagator, while $\rho_{ab}(x, y)$ is related to the spectrum of the theory. Before moving to the results, it is necessary to specify a set of initial conditions.

2.4 Saddle solution as initial condition

Appropriate initial conditions to numericcally simulate (2.17) are necessary. Our goal is clear: we wish to study how the classical unstable condensate evolves as quantum fuctuations are dynamically taken into account. Therefore, a natural choice is to consider, at $t = 0$, the classical condensate solution. That means that, initially, the field ϕ is fixed by the stationarity condition

$$\frac{\delta S[\phi]}{\delta \phi_a} = 0 \quad (2.21)$$

while, for the propagator G , we need to invert the following operator

$$G_{ab}^{-1}(x, y) = i \left(\left(\partial^2 + m^2 + \frac{\lambda}{4} \phi_a^2 \right) \delta_{ab} + \frac{\lambda}{2} \phi_a \phi_b \right) \delta^{(2)}(x - y). \quad (2.22)$$

This is already done in [10], and leads to

$$\begin{aligned} \tilde{G}_{ab}(t - \tau, x - y) &= \frac{1}{L} \int \frac{d\gamma}{2\pi} \sum_{n=-\infty}^{+\infty} e^{-i\gamma(t-\tau) + ip_n(x-y)} \tilde{G}_{ab}(\gamma, p_n) \Big|_{p_n = \frac{2\pi n}{L}}, \\ \tilde{G}_{ab}(\gamma, p_n) &= \frac{i \left(\left(\omega^2 + \gamma^2 - p_n^2 - m^2 - \frac{\lambda}{4} f_d^2 \right) \delta_{ac} + 2i\omega\gamma\epsilon_{ac} - \frac{\lambda}{2} f_a f_c \right)}{\left(\gamma^2 - \gamma_+^2(p_n) + i0 \right) \left(\gamma^2 - \gamma_-^2(p_n) + i0 \right)}, \end{aligned} \quad (2.23)$$

where the relation between G , \tilde{G} and ϕ , f is given by

$$\begin{cases} \phi_a(t, x) = R_{ab}(\omega t) f_b \\ G_{ab}(t, x; \tau, y) = R_{ac}(\omega t) R_{bd}(\omega \tau) \tilde{G}_{cd}(t - \tau, x - y) \end{cases} \quad (2.24)$$

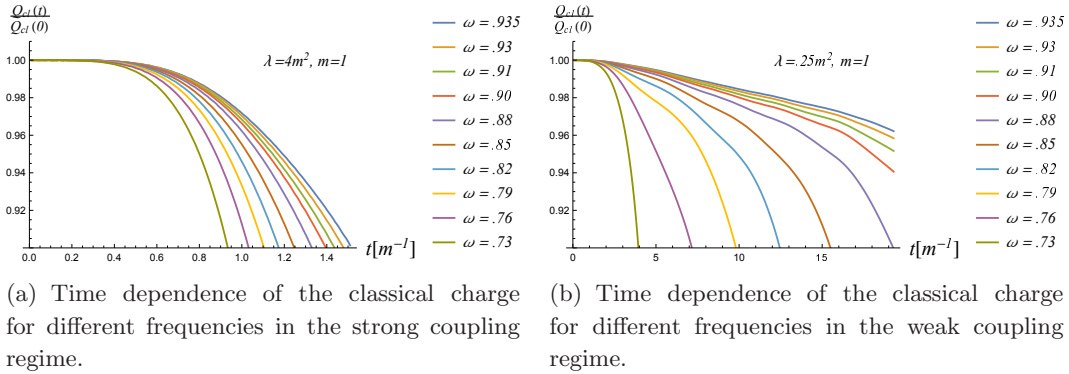


Figure 3. Time evolution of classical charges

with $R_{ab}(\theta) \in SO(2)$ the standard rotational matrix, f amplitude fixed by condition (2.4) and $\gamma_+(p)$ and $\gamma_-(p)$ are defined in (2.7) and (2.8). Since for the tree level solution $\gamma_-(0)$ is gapless and $\gamma_-(p_1)$ has imaginary part, in order to specify initial conditions for F from (2.23), at $t = 0$, the zeroth and first momentum modes of the statistical propagator were removed. This corresponds to move slightly away from the saddle point, anyway without affecting the dynamics in a relevant way. The mapping of the initial conditions between G and F and ρ is explicitly derived in [10].

3 Numerical Analysis

In the following we discuss our numerical results.

Eq.s (2.17) have been solved numerically using the Crank-Nicolson finite difference scheme for derivatives, and a trapezoidal rule for memory integrals. Moreover, since we are interested in the region where the classical spectrum is splitted between the condensate and the bright soliton, we confine our study to the range $\omega \in (\omega_{cusp}, \omega_{cr})$ ³. In this region, our choice of initial conditions, namely the unstable condensate solution, leads to the presence of one imaginary mode. As L is increased, more and more modes display such behaviour in the above-mentioned ω range, as it can be easily seen from (2.8). Therefore, the size of the box is purely dictated by reasons of simplicity: first of all the box size should be much bigger than the constituents Compton wavelength ω^{-1} and, secondly, the numerical analysis simplifies a lot if only one instability mode shows up in the explored ω 's range. In view of this, we chose the box size to be $L = 4\pi m^{-1}$, for which $\omega_{cusp} \simeq 0.71m$, $\omega_{cr} \simeq 0.94m$ and only one instability mode is present, namely the first one $\gamma_-(p_1)$. In all the simulations we fixed $m = 1$.

The general behaviour of the quantum breaking is displayed for different ω 's in fig. 3 for strong and weak coupling. The behaviour is very reminiscent to the one observed for the quantum breaking in the repulsive case for a stable condensate [10], although much faster. However, even if not shown explicitly, we notice the following feature: for all the

³To avoid confusion we have to mention that for fixed ω , the charges of soliton and condensate are different and they have, correspondingly, different energies (as it can be seen from (2.6) and (2.14)), though they coincide at the critical point $Q_{b.s.}(\omega_{cr}) = Q_{b.c.}(\omega_{cr})$

simulations in the strong coupling regime, the total charge (1.3) varies on the displayed timescales by approximately the 1% i.e. $Q(m^{-1})/Q(0) \sim 0.99$. This is comparable to the change in classical charge displayed in fig. 3(a). However, due to the coupling being strong, we do not expect the resulting simulation to approximate appropriately the true quantum evolution anyway. The situation is qualitative different in the weak coupling regime fig. 3(b). There, even though the coupling is weak, as ω is decreased (and the collective coupling is increased), there is a violation of the conservation of the total charge. This is, however, practically negligible (at least 100 times smaller and slightly growing with the collective coupling). This is no longer the case as we look at the simulation for longer times. For example, when $Q_{cl}(t) \approx 0.5 Q_{cl}(0)$ we generically notice an increasing violation of the total charge conservation. This underlies a failure of our numerical scheme as the exponential growth of Q_q is so fast that it can no longer be well approximated after certain timescales. We now proceed with the discussion of the two main results of this work.

3.1 Evolution along the BEC trajectory

The first result we wish to comment upon is the evolution of the unstable condensate.

We will introduce here two notions for the energy as we did for the charge. So, in full analogy with $Q_{cl}(t)$ and $Q_q(t)$ defined in (1.4) and (1.5) we define

$$E_{cl}(t) = \int dx \left(\frac{1}{2} (\partial_0 \phi_a)^2 + \frac{1}{2} (\partial_i \phi_a)^2 + V(\phi_a) \right) \quad (3.1)$$

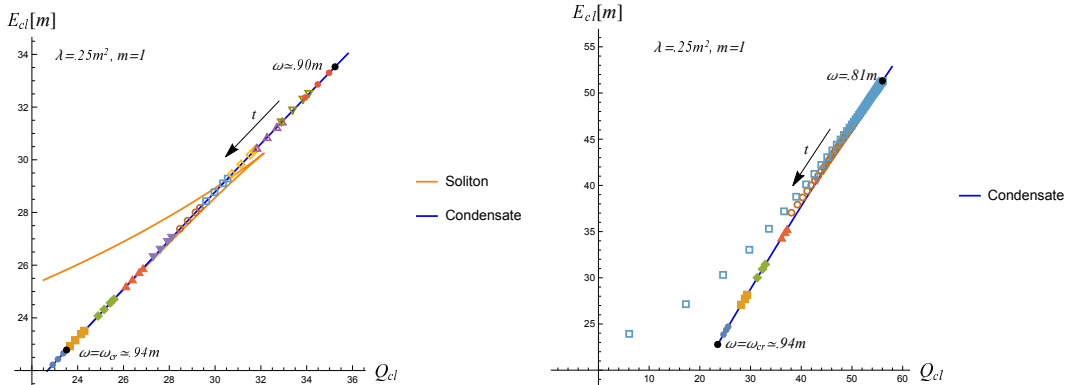
and quantum part which we are not interested in writing explicitly here.

The sum of two is a conserved quantity

$$\frac{d(E_{cl}(t) + E_q(t))}{dt} = 0. \quad (3.2)$$

During the evolution both classical charge and energy diminish while full integrals of motion are conserved. In Fig. 4, the evolution of this classical quantities is shown for different ω 's (different colors) and compared w.r.t. the branch of classical condensate solutions (blue line).

The points in the plot are numerical evaluations of the classical energy (3.1) and charge (2.6) at different times. Different colors there correspond to different initial configurations, namely different initial ω . Therefore looking the dots of particular color, which coordinates at thre plot are $(Q_{cl}(t), E_{cl}(t))$, one can see how the classical energy and classical charge of this configuration evolve with time. In Fig. 4(a) one can see how the numerical simulations fully evolve along the classical condensate trajectory. The reader might wonder why no deviations are seen, although lower energy configurations (at similar charge), namely the soliton (orange line), are present. The reason is that the bright soliton is a localized configuration, and therefore, due to the homogeneity of our initial conditions, the system in principle can only evolve into a superposition of such solutions. We must admit that here we actually do not know how to understand whether initial homogeneous configuration is tending to approach a superposition of solitons or not but there is a clear qualitative picture explaining the condensate evolution along the BEC $E_{cl}(Q_{cl})$ line.



(a) Time evolution of the classical energy $E_{cl}(t)$ as a function of $Q_{cl}(t)$ for different $\omega \in (.90, \omega_{cr})$ (each with a different marker). Here the evolution follows the classical condensate trajectory.

(b) Time evolution of the classical energy $E_{cl}(t)$ as a function of $Q_{cl}(t)$ for different $\omega \in (.81, \omega_{cr})$ (each with a different marker). The failure of the simulation is apparent as ω decreases.

Figure 4. Time evolution of the classical energy as a function of Q_{cl} for different frequencies.

In total analogy with the Q-balls case, one can deduce the following relation between classical energy and charge of the BEC

$$\frac{dE_{cl}}{d\omega} = \omega \frac{dQ_{cl}}{d\omega}. \quad (3.3)$$

Therefore, one can conclude that if classical charge is getting changed by some small amount δQ_{cl} , which in our case the part carried out by fluctuations, then the next homogeneous configuration stationarizing the local part of the energy is given by

$$E_{cl}(\delta t) \simeq E_{cl}(0) + \omega \delta Q_{cl}(\delta t), \quad (3.4)$$

which means that during quantum evolution, the preferable directions in the phase space is the one stationarizing the classical part as long as classical quantities remain dynamically dominant. This is true as long as $Q_{cl} \gg Q_q$, but in the end, upon reaching t_{qb} , this approximate relation does not need to hold, as well as our \hbar perturbative expansion (See discussion in Sec. 1), and evolution might deviate from this curve. Anyway, we will see in the next paragraph how the presence of a lower energy configuration affects the speed at which the system rolls along the BEC $E_{cl}(Q_{cl})$ trajectory.

The situation is different in Fig. 4(b) where the behaviour of simulations is shown for lower ω 's. As one can see, some of the simulations (blue squares) start deviating from the condensate-like evolution. Such deviations increase as ω decreases. Such phenomenon is analogue to the one observed for the strong coupling case. Namely, the exponential growth becomes so fast, as to lead to a failure of the numerical scheme. In fact, correspondingly with these deviations, non negligible - yet very small - violations of total charge emerge. However, it should be noted that for small timescales, the evolution of these simulations is still reliable.

3.2 Quantum break time

In order to capture the rate at which the system evolves along the condensate trajectory (c.f. Fig. 4), we use criterion (1.6) to obtain t_{qb} . Moreover, because of the above mentioned numerical issues, we fix quantum breaking as the time such that $Q_q(t_{qb}) = 0.1 Q_{cl}(t_{qb})$. In this way, on the obtained quantum breaking timescales, most of the simulations have a very well conserved charge (within .1% deviations). The dependence of t_{qb} on $\log Q/\text{Im}(\gamma_-(p_1))$ is explicitly shown in Fig. 5, where the quantum breaking time is shown w.r.t. ω . One can see how in this coupling region i.e. $\lambda \leq 0.1 m^2$, the breaking time is indeed captured by the relation

$$t_{qb} \simeq \frac{\log Q}{\text{Im}(\gamma_-(p_1))} + \text{constant} \quad (3.5)$$

where $\text{Im}(\gamma_-(p_1))$ is the Lyapunov exponent, therefore confirming (1.2) mentioned in the introduction. Let us discuss this relation and the corresponding physics in more details.

Firstly, it is very important to stress that such a logarithmic behaviour is controlled by the Lyapunov exponent which sets the system instability. As long as a homogeneous solution exhibits this form of instability, the leading initial time behaviour is apparently governed by this mode arising in the Green's function. Therefore we can roughly say that for $\delta t \sim 1/\text{Im}(\gamma_-(p_1))$

$$Q_{cl}(\delta t) \simeq Q_{cl}(0) + A \left(1 - e^{\text{Im}(\gamma_-(p_1))\delta t} \right) \quad (3.6)$$

and we can infer from this, that using our quantum breaking criterion $Q_{cl}(t_{qb})/Q_{cl}(0) \simeq r$, we obtain (3.5). Indeed, the aforementioned constant in (3.5) depends only on the chosen criterion r and is almost independent on any parameters of the model.

From the quantum point of view, this law means that to undergo quantum breaking, the system has to wait for a significant amount of quanta to decay, which leads to logarithmic dependence of quantum break-time on charge. This mechanism is in contrast with the classical picture, where departure from stationary solution is set by inhomogeneities introduced by means of initial classical perturbations. To clarify this difference let us briefly recap how the decay due to classical perturbations takes place. In fact, for this to happen, the inhomogeneous perturbation spectrum needs to include an unstable mode, which, in the system under consideration, corresponds with the first momentum mode. In turn, the presence of such a mode leads to the development of inhomogeneities in the system on a time scale fixed by the lyapunov exponent as $1/\text{Im}(\gamma_-(p_1))$, leading to the localisation of the soliton. Thus, we see that departure occurs almost immediately, independently of the initial configuration itself (namely amount of quanta realising the initial state). This kind of transitions were clearly demonstrated for unstable Q-balls (Q-clouds) as they are perturbed and, after a time-scale set by the instability, they move to a stable configuration, dropping some charge along the process [19]. In addition, we must stress again, that not all the perturbations can destroy BEC classically, but only those which contain the unstable mode. This is totally different from what happened in our case as the evolution is driven by quantum effects preserves translational invariance. In fact, we saw in Fig. 4(a) classical quantities evolve along the classical homogeneous BEC trajectory, although the growth of

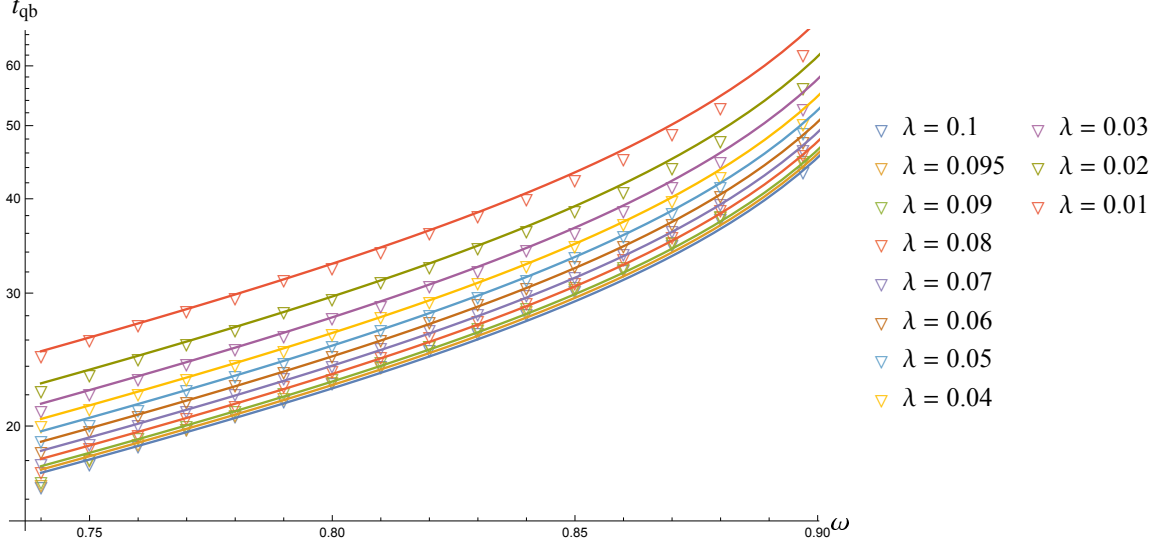


Figure 5. Quantum breaking time dependence on ω compared to analytical estimation. Solid lines are functions $\log Q(\omega, \lambda)/\text{Im}(\gamma(p_1, \omega))$ for different couplings and triangles are quantum breaking times extracted from simulations

the unstable mode within the Green's function being present (note that at $t = 0$ we input this unstable mode to be zero). Therefore, we see that quantum and classical process are significantly different. In particular, the quantum decay is more general as it takes place independently whether or not homogeneity is preserved by initial conditions.

One clear feature of Fig. 5 is the deviation from the logarithmic scaling as the coupling is increased. We believe this to be due to the above discussed failure of the numerical scheme.

4 Conclusions and Outlook

In this work we studied the behaviour of a relativistic BEC near its classical instability. It was found that the quantum break-time, namely the moment when departure from the classical solution become significant, scales logarithmically with charge Q and is controlled by the Lyapunov exponent γ characterising the classically instability of the system, namely

$$t_{qb} = \gamma^{-1} \log Q + C, \quad (4.1)$$

with C a small constant caused by the way we extracted numerically t_{qb} . This result for quantum break-time is similar to the one derived in [7] (see eq. (1.2)). However, being our study in the relativistic regime, we see that the number of constituents is replaced with charge $N \rightarrow Q$ (compare (4.1) with (1.1)). These two results need not to be similar as the the spectrum of the relativistic model is much broader. However, as it follows from our analysis, (4.1) is indeed the natural extension of the result of [7] in the relativistic regime.

To obtain (4.1), we worked within the 2-PI formalism, keeping the second order in loop-expansion, which allowed us to numerically simulate the Minkowski time evolution of

the system. After setting as initial conditions the tree level stationary condensate solution, we introduced a new general criterion to measure its deviation from the classical solution, namely we chose as observable of interest the ratio between Q_{cl} which is the functional of 1-point expectation value and Q_q given by connected part of the propagator evolved in time. A natural criterion to obtain the quantum break time, therefore, relies on the dynamical condition $Q_{cl} \approx Q_q$ (see (1.6)). Such timescale, is what we refer to as t_{qb} in (4.1). This condition, already introduced by us in [10], turns out to be very simple as it requires the measurement of only an integral quantity, to be compared with [7], where t_{qb} was calculated via entanglement arguments. It is therefore quite intriguing that such different methods do agree. Note that such condition might be imposed for any other integral quantity (e.g. energy) as long as its conservation constrains the dynamical evolution of the system. Therefore the criterion introduced in [10] proves general and with a wide applicability range.

Another interesting result of this article is related to the breaking trajectory of the condensate. In fact, the evolution takes place along the branch of classical solution $E_{cl}(Q_{cl})$ as long as charge is steadily getting carried away by quantum fluctuations according to (3.3) and (3.4) (see Fig. 4). There, the classical part of the energy w.r.t. classical charge evolves along the branch of classical solutions given by (2.5) and (2.6). This is due to the fact that homogeneity is preserved in our equations. In fact, as discussed above, there is a preferable direction in the phase space of classical configurations set by (3.3). Indeed, as soon as quantum breaking takes place, we do not expect this kind of relation to hold and the system might evolve differently from there onward. Further investigation of this issue, although interesting, is beyond the scope of this work. Moreover it can be seen that as either the coupling or the collective coupling is increased, deviations from such trajectory are observed in Fig. 4. We believe this to be due to a failure of our numerical scheme. We therefore excluded such simulations when studying the functional dependence of the quantum break time.

In the future it would be interesting to add extra diagrams to our loop expansion or attempt a $1/N$ resummation which would allow us to carry the numerical integration further. Also, another interesting question is how the system evolves when considering as initial conditions the bright soliton configuration (see Fig. 2). In fact, exploring its evolution might help us deepening our knowledge regarding the backreaction properties of localised objects.

Acknowledgments

First of all we would like to thank IMPRS research school of Max-Planck Institute for Physics for giving us the opportunity to participate in their program for PhD students and Arnold Sommerfeld center for having great scientific environment there. As well we are grateful to our supervisor Gia Dvali for inspiring and useful discussions and for reading the manuscript. A. K. wants to thank Emin Nugaev for discussing the results and for useful advises. M. Z. is thankful to Lorentz center in Leiden for its kind hospitality and fruitful discussions he had there while working on the project.

References

- [1] G. Dvali and C. Gomez, *Black Hole's Quantum N-Portrait*, *Fortsch. Phys.* **61** (2013) 742–767, [[arXiv:1112.3359](#)].
- [2] G. Dvali and C. Gomez, *Black hole macro-quantumness*, *arXiv preprint arXiv:1212.0765* (2012).
- [3] G. Dvali and C. Gomez, *Black hole's 1/n hair*, *Physics Letters B* **719** (2013), no. 4-5 419–423.
- [4] G. Dvali and C. Gomez, *Quantum compositeness of gravity: black holes, ads and inflation*, *Journal of Cosmology and Astroparticle Physics* **2014** (2014), no. 01 023.
- [5] G. Dvali, C. Gómez, and S. Zell, *Quantum break-time of de sitter*, *Journal of Cosmology and Astroparticle Physics* **2017** (2017), no. 06 028.
- [6] G. Dvali and S. Zell, *Classicality and Quantum Break-Time for Cosmic Axions*, *JCAP* **07** (2018) 064, [[arXiv:1710.00835](#)].
- [7] G. Dvali, D. Flassig, C. Gomez, A. Pritzel, and N. Wintergerst, *Scrambling in the black hole portrait*, *Physical Review D* **88** (2013), no. 12 124041.
- [8] P. Hayden and J. Preskill, *Black holes as mirrors: quantum information in random subsystems*, *Journal of high energy physics* **2007** (2007), no. 09 120.
- [9] J. Berges, S. Borsányi, U. Reinosa, and J. Serreau, *Nonperturbative renormalization for 2pi effective action techniques*, *Annals of Physics* **320** (2005), no. 2 344–398.
- [10] A. Kovtun and M. Zantedeschi, *Breaking bec*, *arXiv preprint arXiv:2003.10283* (2020).
- [11] J. Schwinger, *Brownian motion of a quantum oscillator*, *Journal of Mathematical Physics* **2** (1961), no. 3 407–432.
- [12] L. V. Keldysh et al., *Diagram technique for nonequilibrium processes*, *Sov. Phys. JETP* **20** (1965), no. 4 1018–1026.
- [13] J. Berges, *Introduction to nonequilibrium quantum field theory*, in *AIP Conference Proceedings*, vol. 739, pp. 3–62, American Institute of Physics, 2004.
- [14] L. D. Carr, C. W. Clark, and W. P. Reinhardt, *Stationary solutions of the one-dimensional nonlinear schrödinger equation. ii. case of attractive nonlinearity*, *Phys. Rev. A* **62** (Nov, 2000) 063611.
- [15] M. Luscher, *Volume Dependence of the Energy Spectrum in Massive Quantum Field Theories. 2. Scattering States*, *Commun. Math. Phys.* **105** (1986) 153–188.
- [16] R. Kanamoto, H. Saito, and M. Ueda, *Quantum phase transition in one-dimensional bose-einstein condensates with attractive interactions*, *Physical Review A* **67** (2003), no. 1 013608.
- [17] N. Vakhitov and A. A. Kolokolov, *Stationary solutions of the wave equation in the medium with nonlinearity saturation*, *Radiophysics and Quantum Electronics* **16** (1973), no. 7 783–789.
- [18] R. Friedberg, T. Lee, and A. Sirlin, *Class of scalar-field soliton solutions in three space dimensions*, *Physical Review D* **13** (1976), no. 10 2739.
- [19] A. Panin and M. Smolyakov, *Classical behaviour of Q-balls in the Wick–Cutkosky model*, *Eur. Phys. J. C* **79** (2019), no. 2 150, [[arXiv:1810.03558](#)].

This figure "2point_non-local.png" is available in "png" format from:

<http://arxiv.org/ps/2008.02187v2>